Hindawi
Geofluids
Volume 2022, Article ID 9552210, 16 pages
https://doi.org/10.1155/2022/9552210

Research Article

Dynamic Monitoring and Research on the Evolution of the Damage of Weakly Consolidated Coal Floor under Dynamic Pressure Using Distributed Optical Fiber

Chang Liu,[1,2] **Pingsong Zhang**,[1,2] **Duoxi Yao**,[2] **Yutong Tian**,[1,2] **and Yuanchao Ou**[1,2]

[1]*State Key Laboratory of Mining Response and Disaster Prevention and Control in Deep Coal Mines, Anhui University of Science and Technology, Huainan City, Anhui Province 232001, China*
[2]*School of Earth and Environment, Anhui University of Science and Technology, Huainan City, Anhui Province 232001, China*

Correspondence should be addressed to Pingsong Zhang; pszhang@aust.edu.cn

Received 9 September 2021; Accepted 24 February 2022; Published 19 March 2022

Academic Editor: Zhijie Wen

During the extraction of coal seam, the evolution pattern of the rock is an important element for controlling the rock seam and preventing water damage to mine. In order to obtain the deformation and damage of weakly cemented coal seam footings under dynamic pressure, the stability of the footings was studied using a combination of various methods, including rock mechanics testing, field testing, and numerical simulations. By sticking distributed optical fiber on the surface of rock samples, the degree and location of rupture on the surface of rock samples could be obtained using the strain response correlation for optical fiber. Two monitoring holes were arranged in the bottom plate of coal seam at 12307 working face of a mine in Ordos Basin, China. Moreover, a distributed optical fiber sensor was implanted in the hole. The results show that the failure depth was 16.5 m. On the other hand, the numerical simulation results show that the failure depth of the bottom plate was 16.0 m, which agreed well with the measured value. The distribution characteristics of the maximum principal stress of the bottom slab during the advancement of working face were obtained using three-dimensional (3D) numerical model. Based on the distributed optical fiber strain tests in the two boreholes in the same vertical profile and combined with the natural proximal interpolation method, the interhole strain increment distribution profile was obtained. The research results provide a reference for the safe mining of coal resources and the prevention and control of water damage in the mine floor.

1. Introduction

The stress concentration caused by coal seam mining can lead to the redistribution of regional rock stress, which in turn leads to changes in the stress state of the coal seam floor rock, deformation, damage, and movement [1]. In the hundreds of meters deep quarry space, the rock material has the characteristics of nonhomogeneity, irregularity, and anisotropy. Coupled with the complex geological conditions and hydrogeological conditions, the deformation and breakage of surrounding rock under dynamic pressure may result in the development of hydraulic fissures and the destabilization of the bottom water barrier to induce sudden water, which poses a great threat to safe and efficient mining of coal mines [2]. The distribution of stress-strain field and the deformation characteristics of the bottom slab rock are one of the primary conditions for studying the depth and extent of damage of the bottom slab. Therefore, monitoring the variations in the geophysical field of coal seam bottom slab and mastering the damage characteristics of bottom slab during coal mining are important elements of mine containment and water damage prevention [3].

At present, many scholars have conducted a lot of research on the evolution of mining damage in coal seam floor. Theoretical studies by Meng et al. [4] obtained the mechanical analytical correlation of any point of the bottom plate by establishing the mechanical model of the bottom plate. Wang et al. [5] considered the stress characteristics of the strike and tendency of the working face and established a spatial semi-infinite body model. They also deduced

the iterative correlation for calculating the vertical stress of the bottom plate. Lu et al. [6] established the mechanical model under the joint action of mining and confined aquifer and obtained the distribution of vertical stress, horizontal stress, and shear stress along the strike of stope floor. Considering the influence of mining pressure and nonuniform hydraulic pressure, Liang et al. [7] proposed two-dimensional hydromechanical calculation model and key layer stability analysis model. By solving for the analytical solution, the methods could help in studying the failure depth and failure characteristics of coal seam mining floor. However, the stope environment is complex, under which, it is difficult to comprehensively consider all the factors. The analytical solution is helpful in studying the damage depth and damage characteristics of the coal seam mining floor. However, the complex environment of the mining site makes it difficult to consider all variables in a comprehensive fashion. Liu et al. [8] conducted numerical simulations on the failure characteristics of the floor of 3306 working face to determine the sensitivity of each major factor that contributes to the failure depth of the floor. Kmab et al. [9] used RFPA (rock failure process analysis) that considers the heterogeneity of the coal rock to simulate the progressive failure process of coal seam floor during mining. Zhang et al. [10] implanted distributed optical fiber sensors in the material model to detect the characteristics of the strain response during mining. Du et al. [11] implanted distributed optical fiber and FBG in the roof of the model and analyzed the deformation and failure of overburden according to the parameter response characteristics. Based upon customized confined water simulation equipment, Jiang et al. [12] conducted similar simulation tests on the fracture and instability characteristics of the roof and floor of the mining face above the aquifer and obtained the variation patterns of the stress of the roof and floor during the mining process. Compared with the field test, the similar model has the features of easy operation, short time consumption, and outstanding effect. Most of the existing similar models are mainly the two-dimensional models, whereas only a handful of three-dimensional models are developed due to the limitations of test equipment and sites. Field tests of the deformation damage of the quarry rock include seismic wave lamination method [13], microseismic monitoring method [14], high-density electrical method [15], and borehole television [16]. Field testing is the most direct testing method to capture the deformation of a rock and the damage under complex geological environment and variables.

In recent years, fiber optic sensing technology has found its way into geological hazard monitoring due to its high accuracy, insulation, and anti-interference features. The technology has been used to monitor the development of the fracture of surrounding rock and accurately reflect its deformation characteristics according to the correspondence between the fiber optic strain and the rock collapse movement [17, 18]. The related research only applies the distributed optical fiber sensing technology to the stope rock stratum test, which cannot be used to comprehensively study the response characteristics of strain to rock stratum deformation and fracture process. Based on distributed fiber, the rock mechanic test is used to compare the deformation and failure stages of rock samples with the fiber strain data. The results provide basis for the analysis and interpretation of field test data. Meanwhile, two one-dimensional borehole datasets in the same plane are combined, and the natural adjacent point interpolation method is used to obtain the two-dimensional strain profile between the layers, which provides a new method for optical fiber data processing. This paper takes the coal seam mining floor in 12307 working face of a coal mine in Ordos Basin (Figure 1) as the research object. Two floor drilling holes are arranged, and distributed optical fiber sensors are implanted in the holes. The disturbance characteristics of coal seam floor rock mass at different depths during the mining process are monitored by drilling distributed optical fiber sensors. Based on distributed optical fiber rock mechanics test, the measured data are analyzed to obtain the mining failure depth of the floor. Meanwhile, the finite difference software, FLAC^{3D} [8], is used to build a three-dimensional (3D) numerical model, whereas further analysis is carried out according to the regional distribution of plastic zone of coal floor.

2. Experiments

The rock uniaxial loading test was performed using the MTS 816 instrument [19]. Figure 2(a) shows the schematic of the testing system and includes loading device, optical fiber, distributed fiber demodulator, jumper, and lighting device. The rock sample was made up of sandstone and obtained from the field monitoring hole with the dimensions of 50 mm × 100 mm (diameter × height) (Figure 2(b)). The loading rate was 0.005 mm/s for strain dynamic testing of uniaxially loaded rock samples. Under indoor conditions, the variation in room temperature was very small, and the effect of temperature on the distributed fiber was negligible.

Figure 3(a) shows the axial strain record of MTS 816. During the first 214 s of loading, the rock sample underwent original pore compression and linear elasticity. When it was loaded to 214 s and the axial pressure became 141.9 kN, local cracks appeared on the surface of the rock sample. The first inflection point appeared in the time axial force curve. During the continuous pressurization of MTS 816, the local fractures were closed. Meanwhile, the rock sample continued to bear, and the bearing pressure continued to increase. When the pressure increased to 279 s and the axial pressure became 134.4 kN, the local cracks of the rock sample were penetrated. The fracture was formed, and the bearing capacity disappeared. The second inflection point appeared in the time axial force curve. The results presented in Table 1 show the whole process. Figure 3(b) shows the cloud diagram of distributed optical fiber test results. It can be seen that, before the formation of local fractures, the microstrain increment of rock sample became positive, and the optical fiber accumulated large tensile strain. After the local cracks were generated, the energy at the fracture position was released, and the strain value decreased. Based upon the previous high increment in strain, it suddenly dropped and even appeared to have negative value. After continuous pressurization, the fracture was closed, and the rock continued to

Figure 1: Geographical location of the study area.

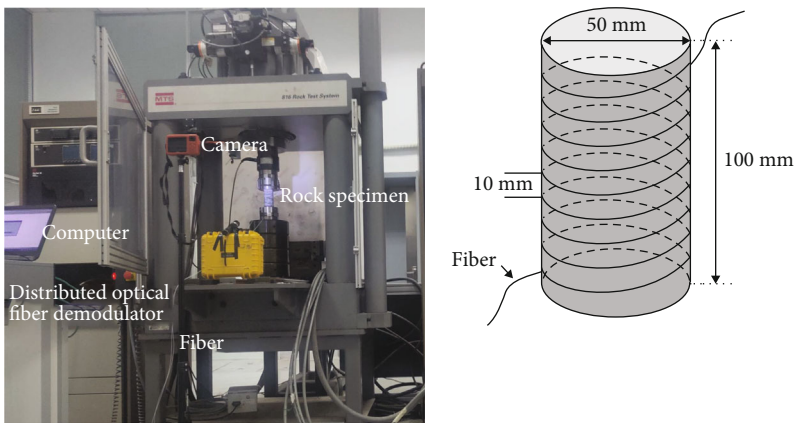

(a) (b)

Figure 2: Schematic of the testing system (a) and rock sample and fiber winding method (b).

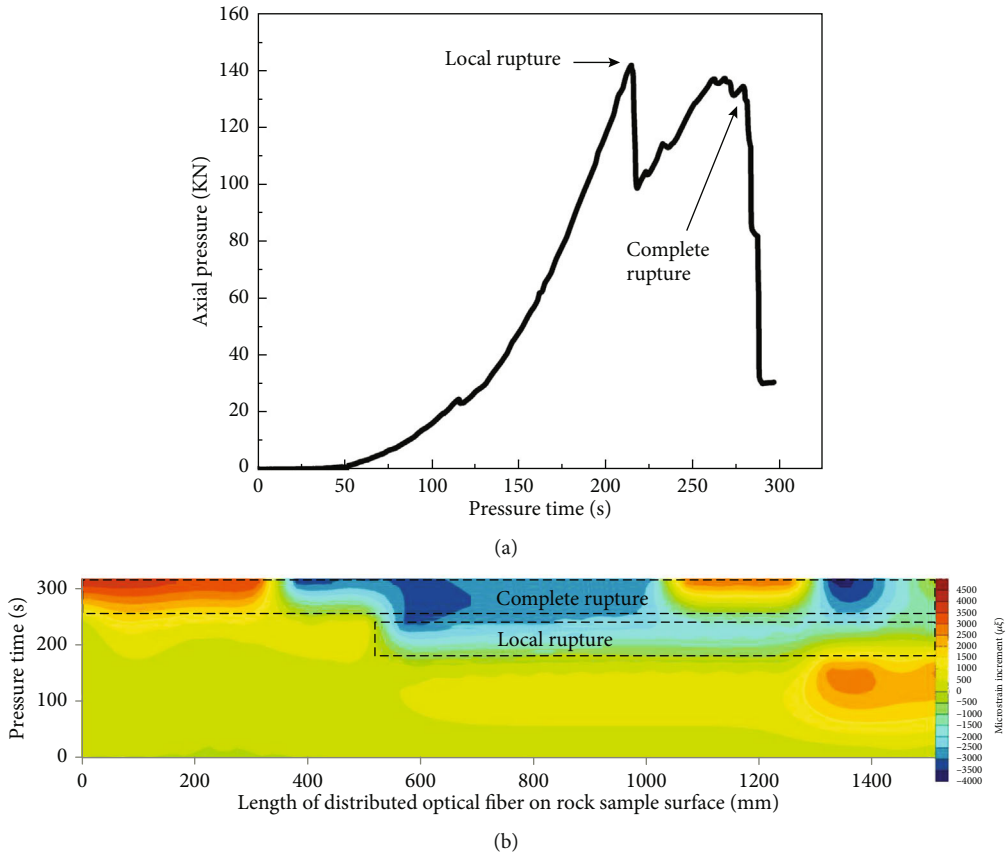

Figure 3: Pressure time-axial stress curve of MTS 816 (a) and strain evolution nephogram of axially pressurized distributed optical fibers (b).

Table 1: Loading process of the rock samples.

Loading time (s)	Axial pressure (kN)	Degree of rock sample damage
0 ~ 214	141.9	Initial pore compression and linear elasticity stages
214~279	98.8 ~ 134.4	Local fissures
>279	<134.4	Completely destroyed

bear until it was completely destroyed. At this time, the energy accumulated by the rock sample was completely released. Combined with the optical fiber strain increment nephogram, the strain increment had a second obvious change, indicating the characteristics of rock fracture.

The strain burst observed by distributed optical fiber corresponded clearly to the spatial spread of cracks on the specimen surface, which could reasonably circle the location of the area where rock damage occurred and sensitively capture the information of rock rupture precursors.

3. Numerical Simulation

3.1. Engineering Geology Overview. Figure 4 shows the spread of the mining area. Mining is mainly conducted in 3-1 coal seam, which belongs to the upper 3 coal group of the Jurassic Middle and Lower Eolian section. The geological conditions of the coal seam in this working face are relatively simple. The thickness of the coal seam in the working face varies greatly, and the average thickness of the coal seam mined in the retrieval range is about 2.2 m. It is a near-horizontal coal seam, and the dip angle of the stratum is 0 ~ 2°. The coal seam is black, with black-brown stripes and dull luster, dominated by dark coal and silk charcoal, and contains a small amount of bright coal with exogenous fissure development. The direct bottom of its bottom plate is sandy mudstone with more developed fissures, and the old bottom is siltstone. The substrate as a whole consists of weakly cemented rock layer. No large fractures and folding structures are found in the area. However, vertical microfissures are developed, which make the back mining face prone to sudden water threat.

3.2. Numerical Model. According to the stratigraphic division of the study area and the comprehensive bar chart of the borehole (Figure 4), the mechanical parameters of the bottom slab rock were obtained using indoor rock mechanics tests (Table 2). The numerical calculation model was

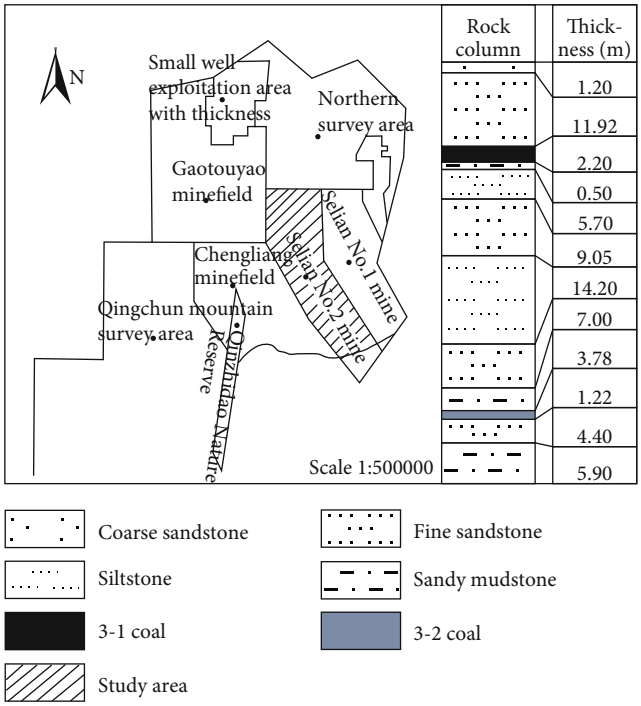

Figure 4: Location of the mining area and stratigraphic lithology histogram.

established, as shown in (Figure 5). Surrounding pressure was applied to the model, and all calculations were completed using the generalized Mohr-Coulomb damage criterion [20]. Mohr-Coulomb theory is more in line with the fracture mechanism of mine surrounding rock and can accurately reflect the mining failure depth of coal seam floor.

As shown in Figure 5, the model was 300 m long in the x -direction, 360 m wide in the y-direction, 80 m high in the z -direction, and 2.2 m thick in coal seam. The 3D model was divided into 206719 units and 194400 nodes. The mechanical boundary conditions of the model are as follows: the fully constrained boundary conditions are adopted at the bottom. The free boundary is adopted at the top of the model, and the surface force is applied to replace the rock stratum that cannot be simulated by the model. Free boundary condition is adopted for coal seam roof. The front, rear, left, and right boundaries of the model are fixed in X and Y directions.

3.3. Simulation Results and Analysis. By simulating the process of advancing the working face along the strike, the cloud diagram of the maximum principal stress distribution and the variation trend of the range of plastic zone affected by disturbance at different depths of the coal seam floor are studied. The variation patterns of deformation and damage to the bottom slab during mining are summarized. The simulation process and the corresponding results are shown in Figure 6.

As can be seen from Figure 6, with the advance of the working face, the maximum principal stress of the floor strata of coal seam was affected by abutment pressure, and the value of the maximum principal stress changed accordingly. The 0 ~ 10 m in front of the work was significantly affected by the advance bearing pressure, and the surrounding rock appeared to undergo stress concentration, which is similar to the conclusion on the stress distribution in the front of the work obtained by Liang [21]. During the mining process, the maximum principal stress in the stress concentration area reached -22.1 MPa. The area below the goaf was a pressure relief area, and with the advancing of the working face, the pressure relief area gradually increased, and the rock stratum produced large deformation after unloading. There was a large range of tensile stress area in the floor of goaf, and the integrity of the rock stratum in the floor of goaf was damaged, which resulted in a continuous increase in the tensile stress area. The floor rock stratum in goaf changed from initial shear failure to tensile bending failure. With further intensification of stress concentration, the tension bending failure occurred in the floor strata of goaf. The distribution of maximum principal stress reflected the failure pattern of floor rock stratum to a certain extent [22].

Figure 7 shows the distribution of bottom plate's failure plastic areas with different excavation distances. It can be seen that, under the action of advance support pressure, the floor rock stratum mainly underwent compression shear plastic failure, and tension failure occurred in the front of the work. With the mining of the working face, the rock mass of the floor of the goaf underwent tensile failure under the action of unloading, forming a certain range of active plastic area. The mining fissures increased with the continuous advancement of the working face, and the failure range of the rock mass increased. There were positive and negative shear stress variation zones in the rock mass under the floor near the elastic-plastic junction at both the ends of the working face. The existence of the shear stress variation zones could promote crack propagation and form compression shear or tension shear failure. This is similar to the conclusion of floor damage obtained by Li [23]. The collapse of the upper strata of the coal seam and recompaction of the goaf weakened the unloading effect of the floor rock mass, so that the development of the floor fault zone slowed down until it completely stopped. At the end of the excavation, the results of plastic zone show that the maximum failure depth of the bottom plate was 16.0 m, while its failure boundary was shear failure mode.

4. Technology Principle

4.1. BOTDR Principles. Fiber optic sensing technology is a direct, continuous, real-time monitoring of the physical parameters at the location of the fiber and makes use of geometrically one-dimensional characteristics of the fiber and the Brillouin scattered optical power frequency shift with the measured temperature or strain parameters as a function of the fiber position length. The effect of strain and temperature on the Brillouin frequency shift can be expressed using Equation (1) [24].

$$V_B(\varepsilon, T) = V_B(0) + \frac{dV_B(\varepsilon)}{d\varepsilon}\varepsilon + \frac{dV_B(T)}{dT}T, \quad (1)$$

where $V_B(\varepsilon, T)$ represents the Brillouin frequency shift value

Table 2: Mechanical parameters of rock mass in the model.

Lithology	Modulus of elasticity E (GPa)	Modulus of shear G (GPa)	Cohesion C (MPa)	Angle of internal friction ψ (°)	Tensile strength Rm (MPa)	Density Y (kg/m^3)
Coal	7.6	0.6	2.7	31.4	0.35	1460
Siltstone	15.6	2.5	3.1	35.2	1.45	2650
Fine sandstone	15.2	1.52	3.2	36.0	1.65	2675
Medium sandstone	13.7	4.3	3.0	35.4	1.6	2697
Coarse sandstone	12.7	5.8	2.8	34.9	1.55	2705
Sandy mudstone	10.2	2.56	2.9	37.5	1.3	2659

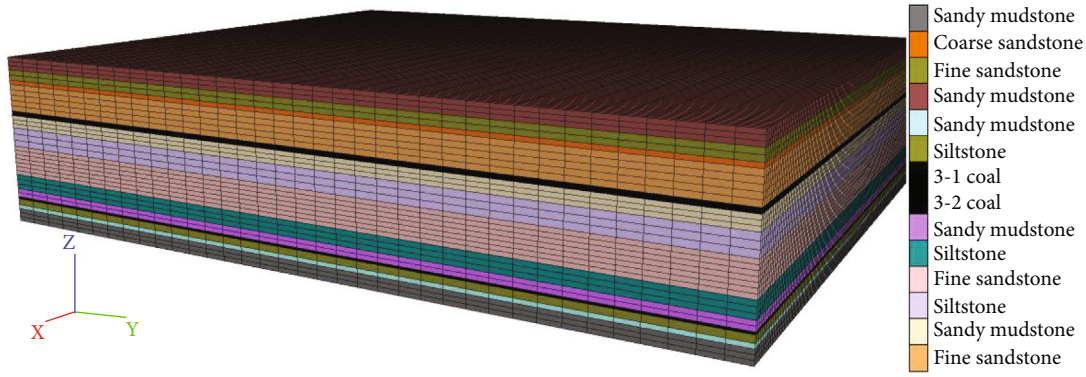

Figure 5: Three-dimensional numerical model.

under temperature and pressure, $V_B(\varepsilon)/d\varepsilon$ represents the Brillouin frequency shift-strain coefficient, $dV_B(T)/dT$ represents the Brillouin frequency shift-strain coefficient, T is the temperature (°C), and ε is the fiber axial micro strain ($\mu\varepsilon$). When the change in test temperature was less than 5°C, the Brillouin frequency shift due to the temperature change could be ignored; however, the Brillouin frequency shift of the fiber axial strain was considered. By measuring the Brillouin frequency shift of the stretched fiber (Figure 8), the strain of the fiber can be obtained by the linear relationship between the amount of change in the frequency shift and the strain of the fiber. Moreover, L represents the distance from the location where scattering occurred to the incident end of the pulsed light. The value of L can be calculated by Equation (2) using optical time domain analysis.

$$L = \frac{ct}{2n}, \tag{2}$$

where c denotes the speed of light in vacuum, n is the refractive index of the fiber, and t is the time interval between the emitted pulsed light and the received scattered light.

4.2. Fiber Optic Strain Test Base Rock Deformation Principle. The distributed monitoring of mining bottom deformation is to implant fiber optic cables in the coal seam and bottom rock. When any deformation occurs in the coal seam, the sensing optical fiber responds to the strain parameters of the bottom rock seam under different mining conditions at the working face. Based upon the results obtained using Equations (1) and (2), the strain value of each point along the sensing optical fiber is obtained. Furthermore, the stress-strain distribution information in the coal seam floor is continuously monitored to realize the dynamic monitoring of the deformation and damage of the floor rock with the progress in the mining process. Additionally, the stress-strain distribution helps in obtaining the state of the development of fracture of the floor or the failure depth of the rock, which provides a basis for mastering the evolutionary pattern of the actual working face floor damage. The outstanding advantage of this monitoring method is that it makes up for the shortage of point monitoring and can obtain continuous distribution information of the measurement in space and time, thus realizing the purposes of real-time, long-distance, and distributed monitoring.

5. Field Testing

5.1. Test Program. The optical fiber testing system was constructed with the help of rock borehole at the bottom of the coal seam. As shown in (Figure 9), the measurement boreholes were arranged at the working face's backwind chute towards the bottom of the roadway. The optical fiber sensors were arranged through the boreholes and drill boreholes downhole. The monitoring hole 1# was at an angle of 13.0°

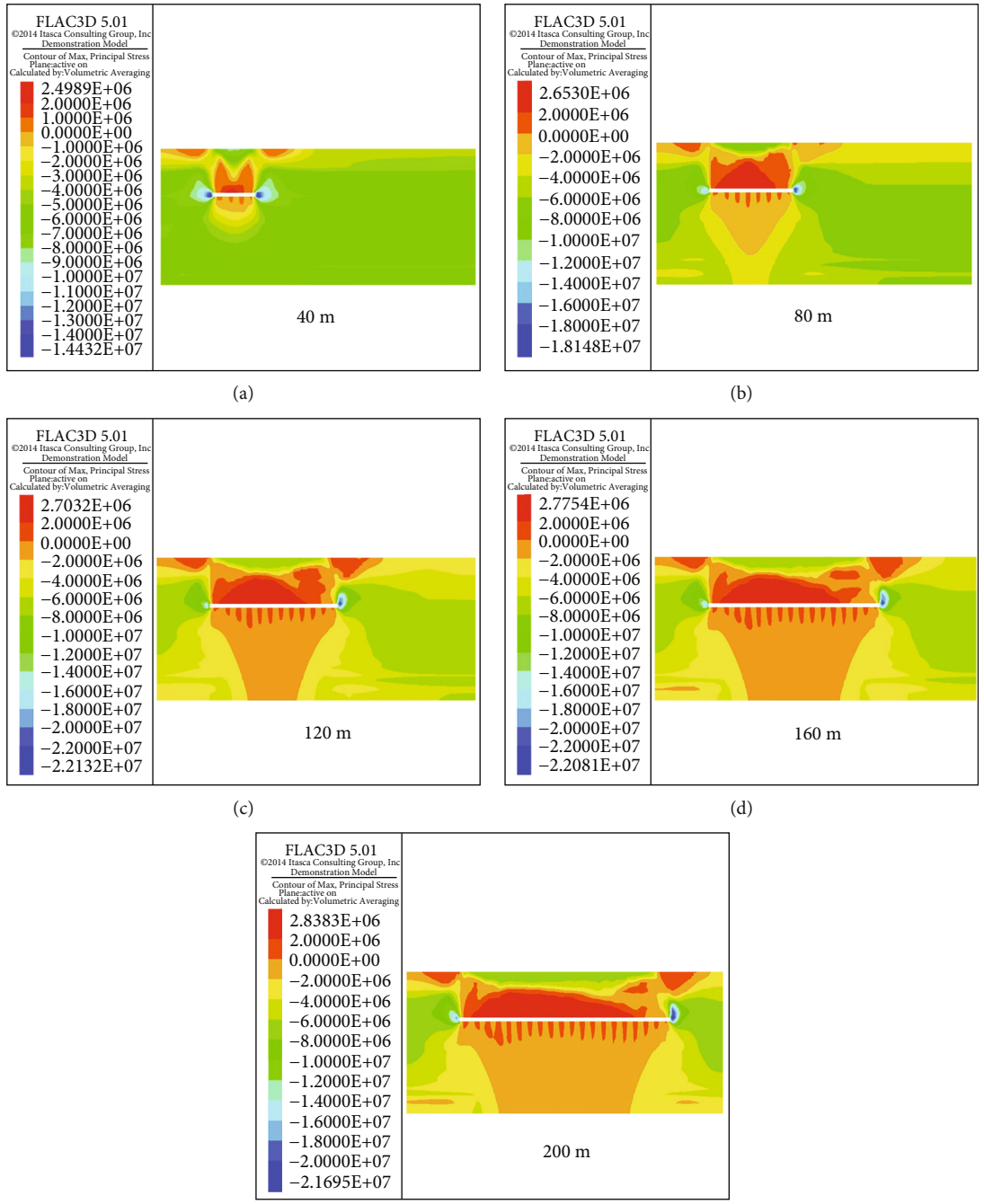

Figure 6: Cloud chart of maximum principal stress distribution at different propulsion distances (unit: MPa).

to the working face, with a depth of 78.0 m and a vertical depth of 17.5 m. The monitoring hole 2# was at an angle of 30.0° to the working face and had the depth and vertical depth of 68.0 m and 34.0 m, respectively. The stress characteristics of the coal seam before and after the mining process were studied, and the data were processed, imaged, and interpreted.

5.2. Analysis of the Results. The on-site data was collated and counted. The collected data from the distance of 97.6 m from the monitoring hole at the retreating footage of the back mining face was taken as the initial value. Furthermore, the variations in the increment in the strain of the optical fiber in holes 1# and 2# were plotted, as shown in Figure 10.

Drill hole 1# was relatively shallow and had a large horizontal length. It was affected by mining before drill hole 2#. There was an overriding effect of dynamic pressure on the rock formation, and the nonlinear response characteristics of rock deformation in the bottom slab were generally inversely related to the depth of the floor [25]. At the distance of 80 m from the orifice, a slight

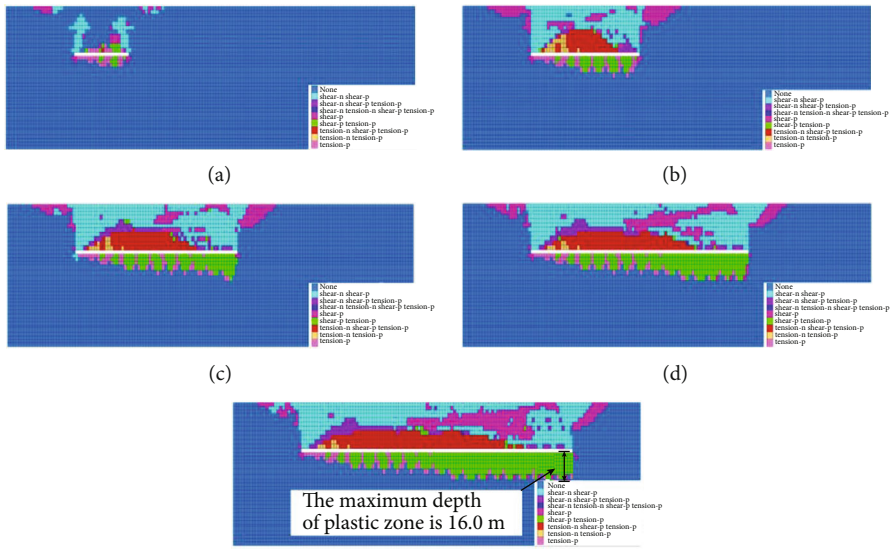

Figure 7: Distribution of plastic zone along the strike in the middle floor of the working face.

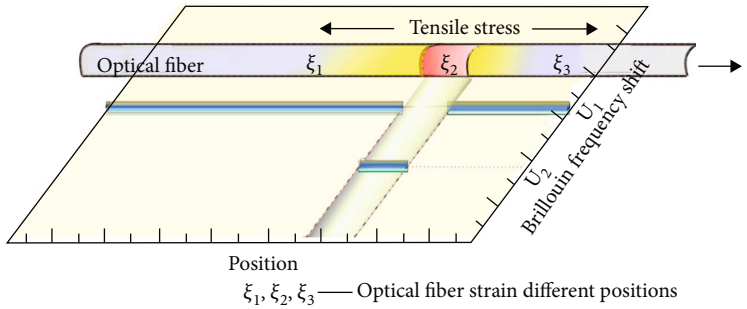

Figure 8: Measurement principle of the BOTDR system.

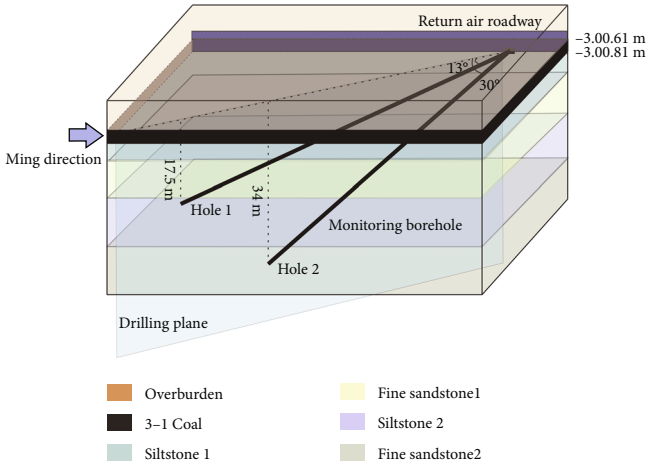

Figure 9: Layout of the monitoring holes.

strain change in the rock layer began to appear. At the distance of 50 m from the hole, the variation in the strain of the rock layer intensified and the local compressive stress of the rock layer increased significantly. Meanwhile, the rock layer started to produce microfractures. When the recovery face was located above the drill hole, the coal mining face showed an increase in the compressive strain, and the rock beneath the mining void showed an increase in the compressive strain. As shown in Figure 10(b), the optical fiber data fluctuated significantly at the hole depth of 33 m, which was analyzed as a rock breaking feature. During the whole process of recovery, when the recovery workface was 33.4 m away from the hole and was located at the vertical depth of -8.4 m in monitoring hole 1#, the maximum value of the pressure-strain increment of monitoring hole 1# was -1098 $\mu\varepsilon$. The tensile strain increased with the maximum value of 893 $\mu\varepsilon$, which is when the retrieval face was directly above the hole and was located at the vertical depth of -7.2 m in the 1# monitoring hole. The maximum value of the increase in pressure-strain in monitoring hole 2# was -2055 $\mu\varepsilon$. At this time, the retrieval face was 48.0 m away from the hole opening and was located at the vertical depth of -16.5 m in monitoring hole 2#. The maximum value of the increase in the tensile strain was 669 $\mu\varepsilon$. Meanwhile, the retrieval face was directly above the hole opening and located at the vertical depth of -15.2 m in monitoring hole 2#. Table 3 lists the maximum values of the distribution of the fiber strain.

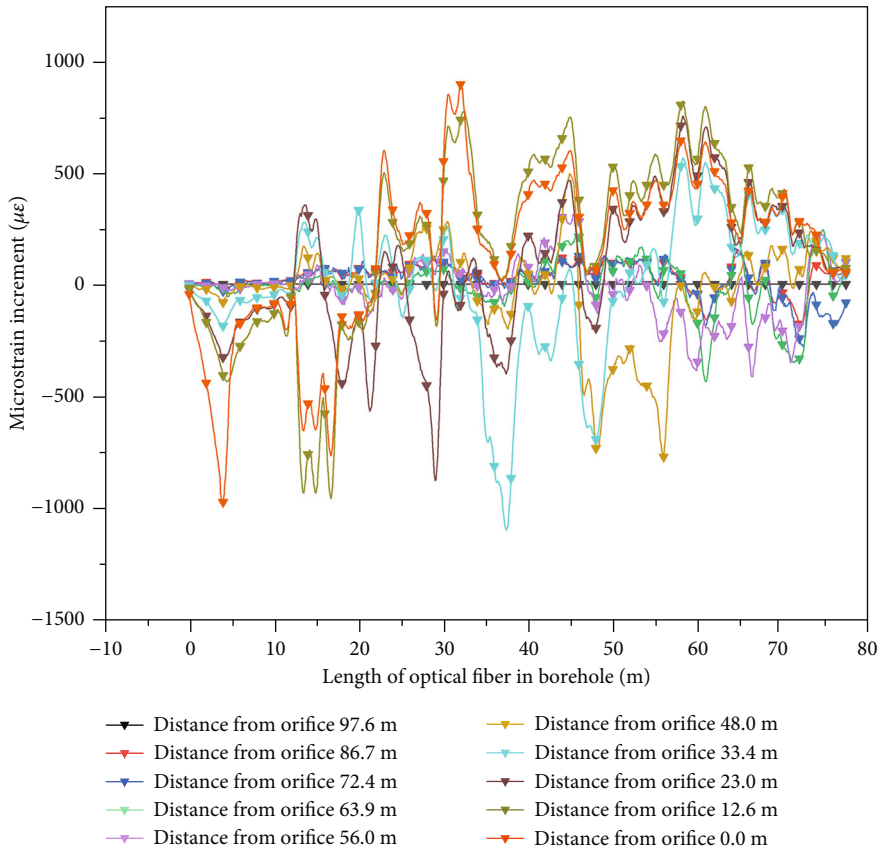

(a)

Figure 10: Continued.

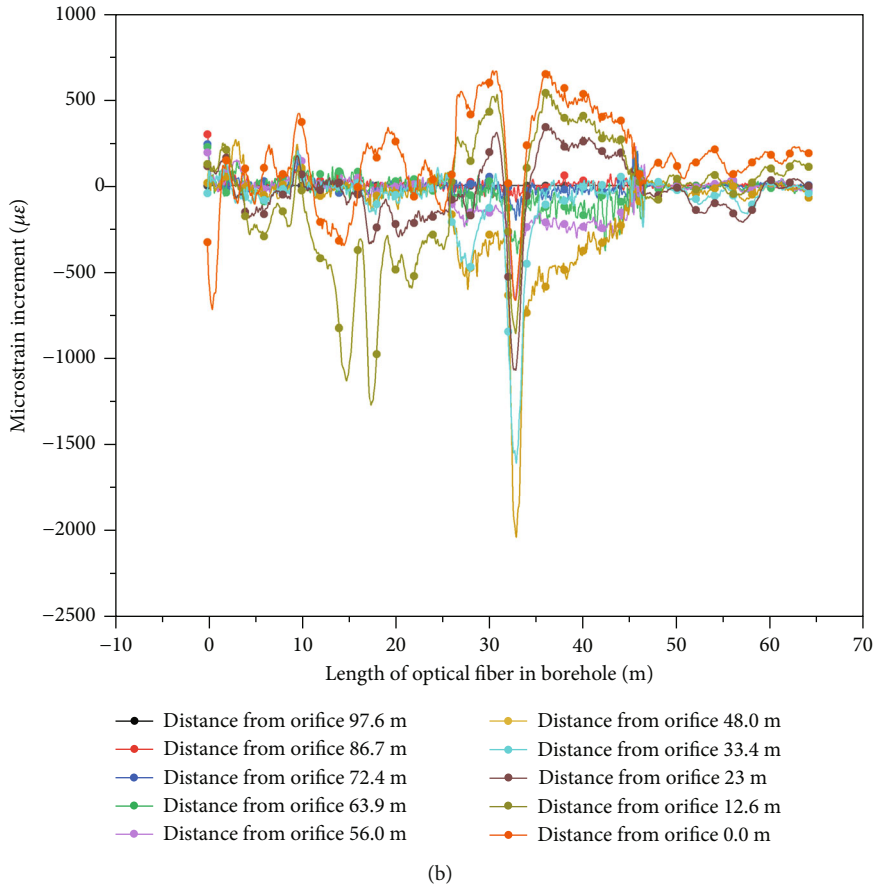

(b)

Figure 10: Optical fiber strain increment curve of hole 1# (a) and optical fiber strain increment curve of hole 2# (b).

Table 3: Distributed fiber strain maximum distribution.

Borehole	Extreme value of strain increment ($\mu\varepsilon$)	Floor vertical depth (m)	Layer	Distance between working face and orifice (m)
1#	-1098	-8.4	Fine sandstone	33.4
	893 $\mu\varepsilon$	-7.2	Fine sandstone	0
2#	-2055 $\mu\varepsilon$	-16.5	Siltstone	48.0
	669 $\mu\varepsilon$	-15.2	Siltstone	0

In order to further analyze the relationship between stress and deformation damage of the bottom slab rock, the relationship between the advancing distance of the working face and the maximum change in strain under different measurement points is shown in Figure 11.

Figure 11 shows the vertical depths of the monitoring points 1 ~ 5 in borehole 1#, which are at the distances of 10.7 m, 13.7 m, 16.2 m, 17.1 m, and 17.4 m, respectively. The monitoring point 1 was located in the middle of the fine sandstone, whereas the support pressure reached its maximum value when the working face was close to the hole opening (at the distance of 33.4 m). After that, the pressure strain value decreased due to the unloading of the mining area. The monitoring point 2 was further away from the hole than the monitoring point 1, and the peak bearing pressure was reached at 63.9 m near the hole, after which the tensile strain increased under the unloading effect of the mining area. The monitoring points 3 ~ 5 were less affected by the process of mining because of their relatively large burial depth, and the reason that their strain changes were relatively small. This indicates that the rock formation where monitoring points 3 ~ 5 were located was relatively stable. Figure 12 takes the vertical depths of monitoring points 6 ~ 10 in hole 2# as 10.5 m, 16.5 m, 18 m, 22.5 m, and 31.5 m, respectively. Except for monitoring points 7 and 10, the peak bearing pressure of monitoring points 6, 8, and 9 were 12.6 m, 23.0 m, and 48.0 m in front of the hole, respectively, which is consistent with the results reported

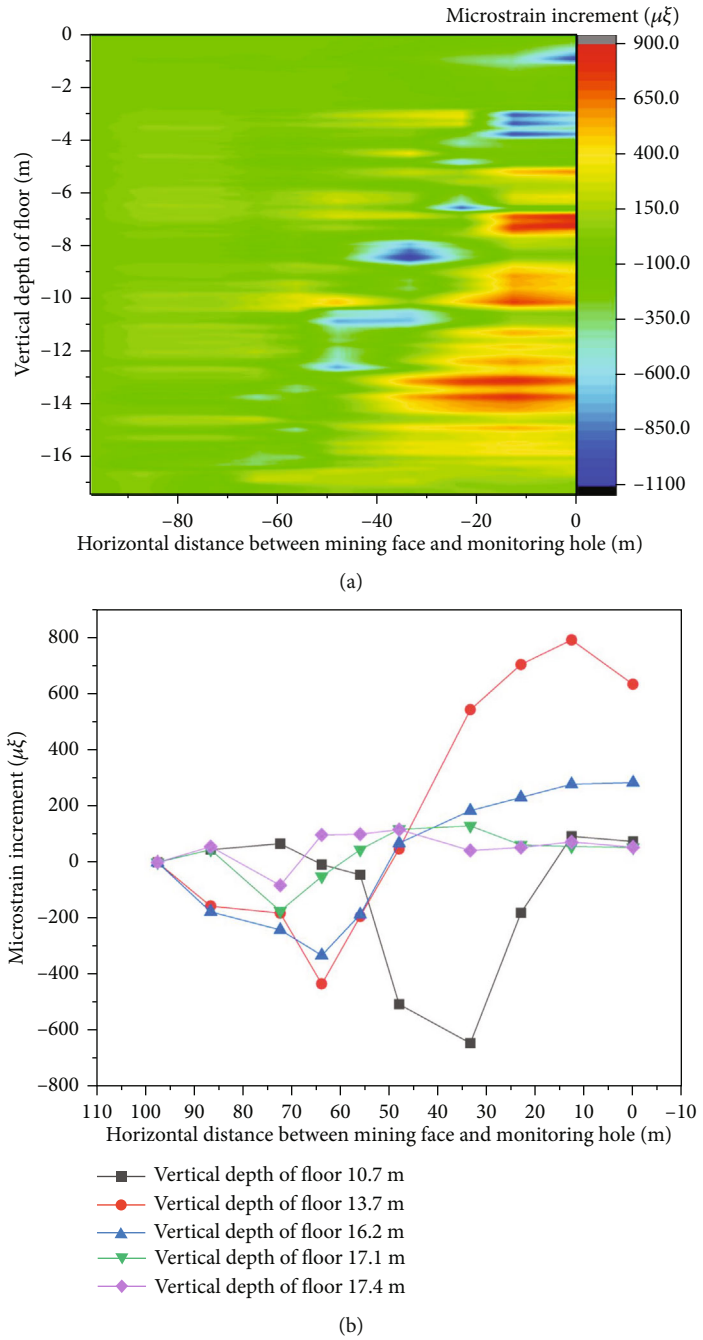

Figure 11: Strain cloud map of hole 1# (a) and strain curve of measuring point in hole 1# (b).

in some previous works [26, 27]. Under the effect of dynamic pressure, with the movement of "shell stress," the peak value of bearing pressure in front of the working face moved forward. This resulted in the peak value of the compressive stress in the borehole near the working face in the monitoring hole and the peak value of stress in the borehole far away from the monitoring point of the working face. The monitoring point 10 was located in the upper part of the fine sandstone formation with a vertical depth of 31.5 m, which remained almost unaffected by mining due to the deeper formation. The increase in peak strain at monitoring point 7 increased steeply from -641 $\mu\varepsilon$ to -2055 $\mu\varepsilon$ at 56.0 m before the hole opening, and the strain recovery under the subsequent unloading of the mining area was also very small, which is in line with the typical characteristics of rock damage that states that the strain changes drastically and in the shape of a "cliff." The strain cannot be recovered after unloading. It can be adjudged that the rocks in this formation had broken and lost their bearing capacity [28, 29].

Based upon a comprehensive analysis, the maximum failure depth of the bottom slab of working face 12307 was 16.5 m. The distributed optical fiber was sensitive to the change of disturbance displacement, had the accuracy of

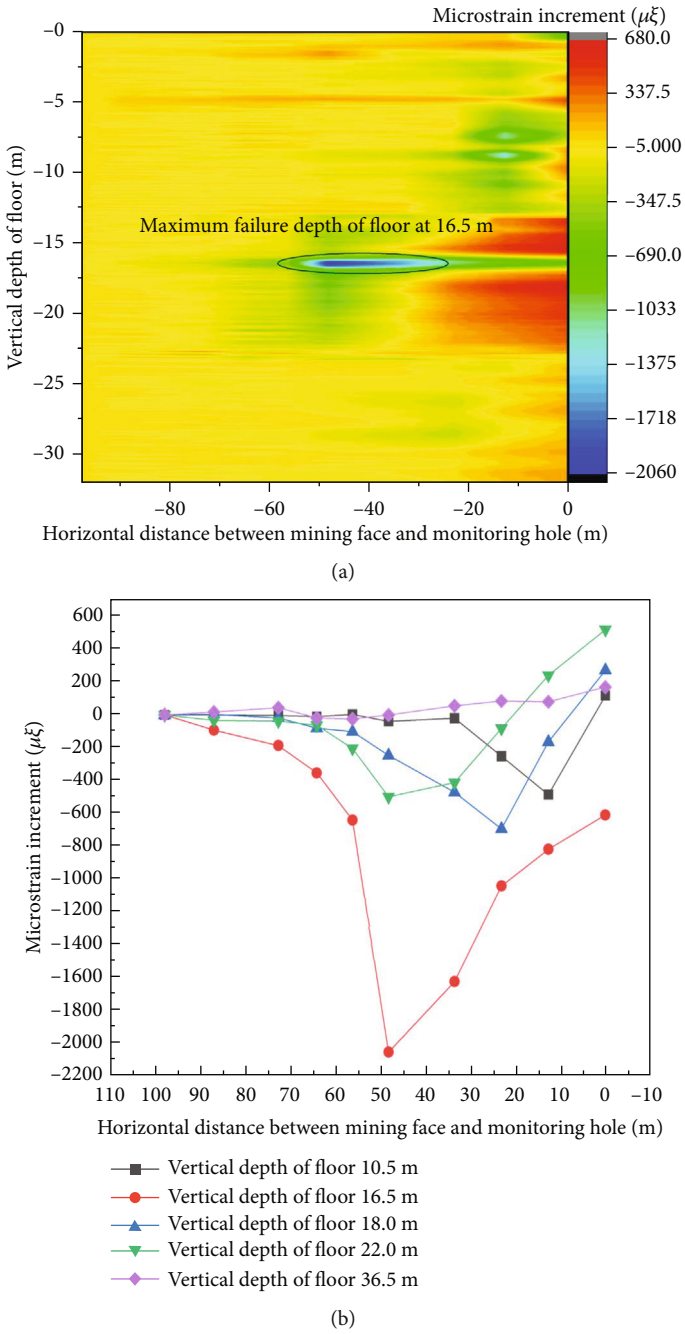

Figure 12: Strain cloud map of hole 2#(a) and strain curve of measuring point in hole 2# (b).

capturing strain data in the borehole, could restore the actual variation pattern of the increase in strain in the monitoring area, and had the capability of realizing the strain change situation of the rock formation in space.

The maximum depth of floor failure is 16.0 m in numerical simulation and 16.5 m in field monitoring, which are similar. According to the research results, key attention should be paid within 16.5 m of the coal seam floor of the working face. Strengthening the floor treatment within this depth range, increasing the number of monitoring boreholes, and reasonable grouting are effective means to maintain the safety of the floor.

6. Discussion

Natural neighbor interpolation (NNI) is one of the most common and effective methods in function approximation theory [30]. NNI is based on computational geometry that is used as the theoretical basis and fully reflects the geometric properties of Voronoi cells and Delaunay triangles and accurately expresses the discrete data [31] between local correlation between the discrete data. Let there be M natural neighbors of point x, which are $p_1, p_2, \ldots, p_M$. The interpolation correlation given by Equation (3) can be constructed. The interpolation results of the point are calculated

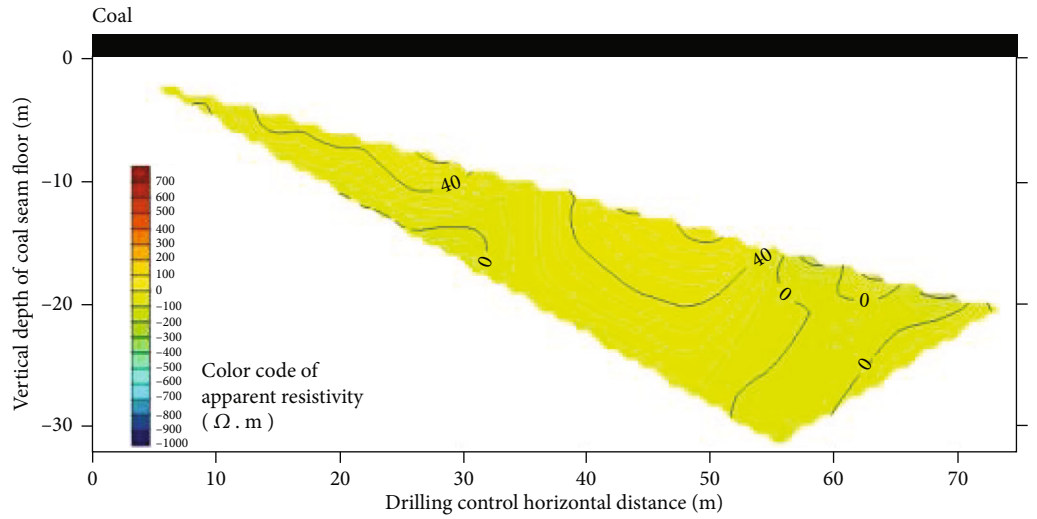

(a)

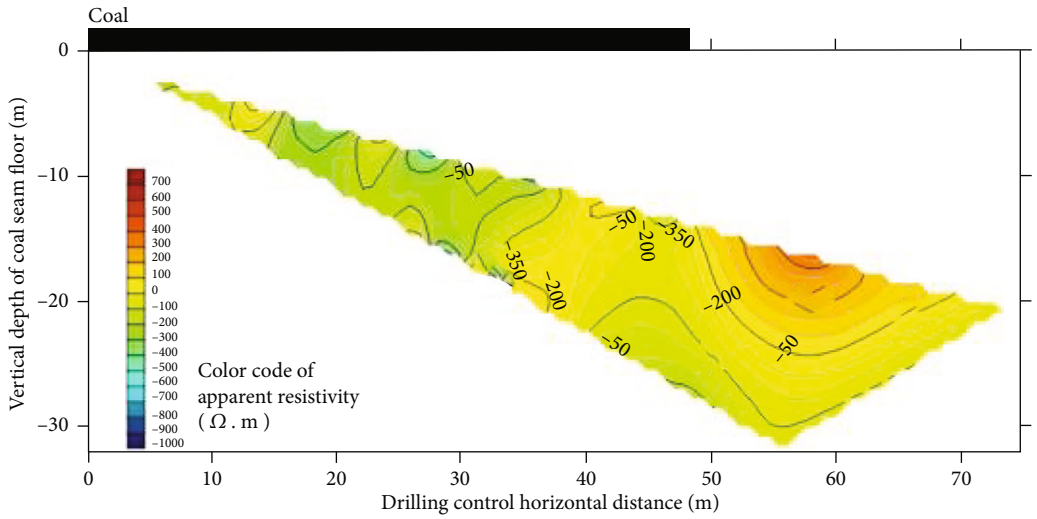

(b)

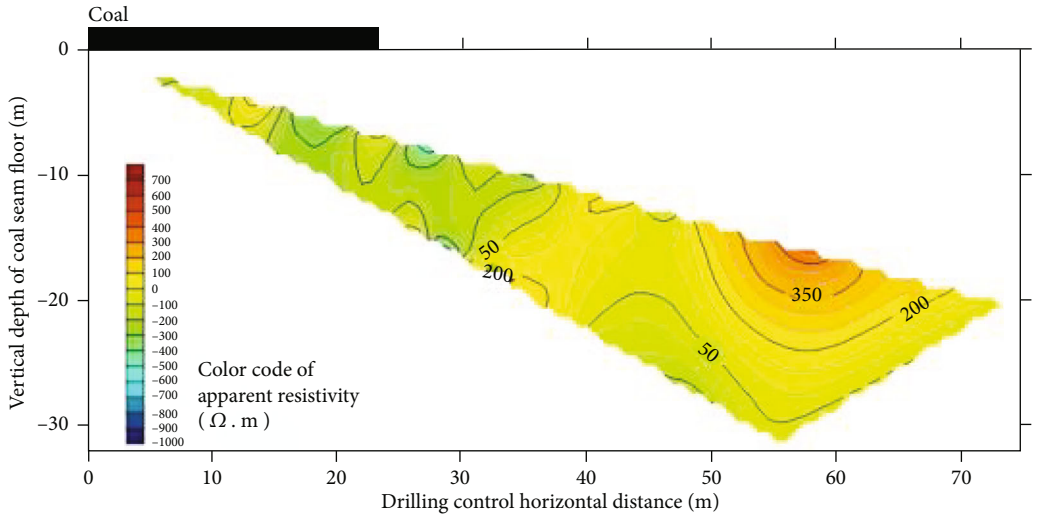

(c)

Figure 13: Continued.

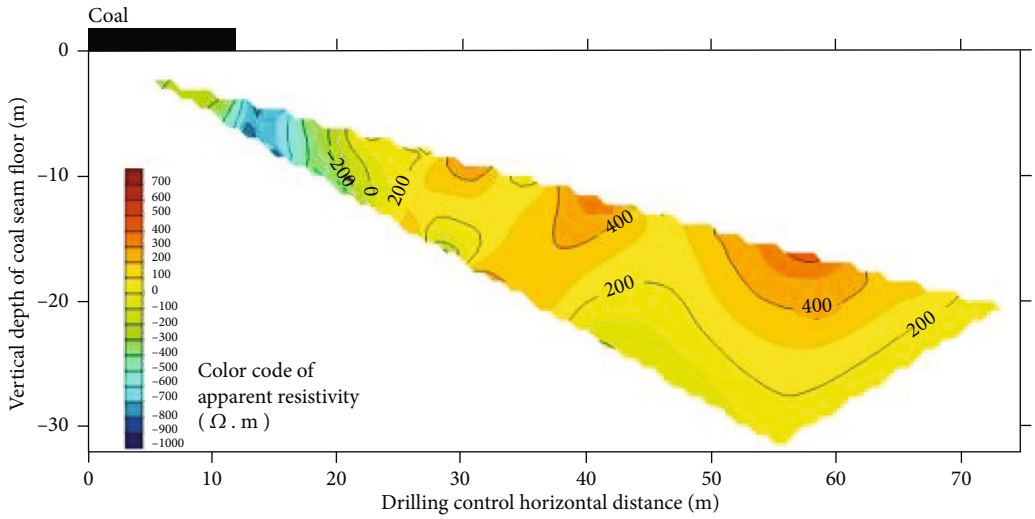

(d)

FIGURE 13: Working face is 86.7 m away from the orifice (a). Working face is 48.0 m away from the orifice (b). Working face is 23.0 m away from the orifice (c). Working face is 12.6 m away from the orifice (d).

according to the rate of contribution of each natural neighbor to point x to be interpolated. It is widely used in 3D geological models containing complex geological phenomena (such as folds, fluids, and force extrusion zones) constructed using boreholes as data sources.

$$f(\mathrm{x}) = \sum_{i=1}^{M} w_i f(p_i), \tag{3}$$

where $f(x)$ is the interpolation result at point x to be interpolated, $f(p_i)$ is the value at the natural neighbor p_i, and w_i represents the weight coefficient occupied by the natural neighbor p_i.

Figure 13 shows the strain data of monitoring holes 1# and 2# into a map using the natural neighbor interpolation method and reflects the distribution of inter-hole strain increment profiles. Initially, the strain in the hole increased slightly. When the mining workface was approaching, the recovery surface was directly above the hole. The compressive stress was concentrated in the bottom plate in front of the workface, whereas the tensile strain increased in the bottom plate below the extraction area. When the mining face was 23.0 m from the hole, the increment in the compressive strain increased significantly, and the rock layer below the working face received extrusion and was influenced by the disturbance. With the emergence of the mining hollow area, the support pressure moved forward. Meanwhile, the rock body in the data characteristics showed the transformation of tensile strain, while the compression and release of rock body under the action of force will result in the development of rock fissures, indicating that the formation of rock structure's deformation and damage. Meanwhile, the upper part of the coal seam collapsed and recompacted the mining hollow area. Furthermore, the unloading effect of the bottom rock body weakened. Therefore, the development of the bottom fracture zone slowed down until it stopped. The characteristics of the two-dimensional joint drilling profile could be a good analysis of the evolution of the bottom-slab rock damage. In the later work, the exploration and application of 3D compositions and new algorithms will be one of the few future research directions.

7. Conclusions

(1) The distributed optical fiber test system was constructed on the rock sample surface based on MTS 816. The cumulative pressurization was 268 s under the displacement control of 5×10^{-3} mm. The distributed strain response results of the whole process of pressurization were obtained. The high-precision strain test of distributed optical fiber sensitively captured the whole process starting from the generation of local fracture to the penetration of the local fracture of the rock. The obtained results provide reference for the analysis of field data

(2) By arranging two monitoring holes with different dip angles at the bottom plate of 12307 to monitor the evolution of the deformation field of the bottom plate under the influence of dynamic pressure, the failure depth of the bottom plate was 16.5 m, which was located near the partition interface of siltstone and fine sandstone. The result was close to the numerical simulation result of 16.0 m, whereas both the techniques adjudged that the failure depth of the coal seam mining floor was 16.5 m. This way, the two verify each other

(3) The three-dimensional numerical model calculated the distribution of the maximum principal stress of the bottom plate and the distribution of the plastic zone of the bottom plate under different excavation distances. The maximum principal stress of the

bottom plate reflected the depth and range of the bottom plate failure. The working face was subjected to stress concentration, and the stress in the goaf was unloaded within a certain range and transmitted to the depth of the bottom plate

(4) Two-dimensional nephogram of strain increment between the monitoring holes 1# and 2# was obtained using natural neighbor interpolation method. The algorithm has advantages in describing the irregular strain change in the floor rock layer, intuitively reflects the distribution characteristics of floor deformation and failure, and provides a novel idea for borehole optical fiber data analysis

Data Availability

The data used to support the findings of this study are available from the corresponding author upon request.

Conflicts of Interest

The authors declare that they have no conflicts of interest.

Acknowledgments

We gratefully acknowledge the financial support by the National Natural Science Foundation of China (Grant No. 41877268 and Grant No. 42074148), the Graduate Innovation Fund Project of the Anhui University of Science and Technology (Grant No. 2020CX2003), and Student Entrepreneurship Fund Support Project of Anhui University of Science and Technology in 2021. We are also grateful to Tian Yutong for her assistance in field testing and data processing.

References

[1] H.-p. Xie, F. Gao, and Y. Ju, "Research and development of rock mechanics in deep ground engineering," *Chinese Journal of Rock Mechanics and Engineering*, vol. 34, no. 11, pp. 2161–2178, 2015.

[2] L. Yuan, "Research progress of mining response and disaster prevention and control in deep coal mines," *Journal of China Coal Society*, vol. 46, no. 3, pp. 716–725, 2021.

[3] Y. Jiang, D. Zhang, K. Wang, and X. Zhang, "Mining-induced damage characteristics of floors during fully mechanized caving mining: a case study," *Advances in Materials Science and Engineering*, vol. 2018, Article ID 1513451, 2018.

[4] X.-r. Meng, C.-h. Xu, Z.-n. Gao, and X.-q. Wang, "Stress distribution and damage mechanism of mining floor," *Journal of China Coal Society*, vol. 35, no. 11, pp. 1832–1836, 2010.

[5] L.-g. Wang, M. Han, Z.-s. Wang, and S.-b. Ou, "Stress distribution and damage law of mining floor," *Journal of Mining & Safety Engineering*, vol. 30, no. 3, pp. 317–322, 2013.

[6] Z.-g. Lu, W.-j. Ju, X.-w. Yin, Z.-y. Sun, F.-d. Zhang, and C.-j. Han, "Mechanism of hard-roof rock burst control by the deep-hole blasting: numerical study based on particle flow," *Shock and Vibration*, vol. 2021, no. 8, p. 14, 2021.

[7] Z.-z. Liang, W.-c. Song, and W.-t. Liu, "Theoretical models for simulating the failure range and stability of inclined floor strata induced by mining and hydraulic pressure," *International Journal of Rock Mechanics and Mining Sciences*, vol. 132, article 104382, 2020.

[8] W. T. Liu, D. R. Mu, L. Yang, L. Y. Li, and C. H. Shi, "Calculation method and main factor sensitivity analysis of inclined coal floor damage depth," *Journal of China Coal Society*, vol. 42, no. 4, pp. 849–859, 2017.

[9] C. Kmab, B. Xysa, and B. Cata, "Floor water inrush analysis based on mechanical failure characters and microseismic monitoring," *Tunnelling and Underground Space Technology*, vol. 108, article 103698, 2020.

[10] D. Zhang, J. Wang, P. Zhang, and B. Shi, "Internal strain monitoring for coal mining similarity model based on distributed fiber optical sensing," *Measurement*, vol. 97, pp. 234–241, 2017.

[11] W.-g. Du, J. Chai, D. Zhang, and W. Lei, "Application of optical fiber sensing technology in similar model test of shallow-buried and thick coal seam mining," *Measurement*, vol. 181, article 109559, 2021.

[12] Z. Li, Z. Changzhi, H. Xie, and F. Yang, "Similar simulation test for breakage law of working face floor in coal mining above aquifer," *Chinese Journal of Rock Mechanics and Engineering*, vol. 30, no. 8, pp. 1571–1578, 2011.

[13] Z.-l. Mu, G.-j. Liu, J. Yang et al., "Theoretical and numerical investigations of floor dynamic rupture: a case study in Zhaolou Coal Mine, China," *Safety Science*, vol. 114, pp. 1–11, 2019.

[14] W.-l. Zhang, T.-h. Huo, C. Li, C.-w. Wang, X.-c. Qu, and C.-w. Xin, "Characteristics of valuable microseismic events in heading face of an underground coal mine using microseismic system," *Shock and Vibration*, vol. 2021, no. 1, p. 10, 2011.

[15] R.-x. Wu, Z.-a. Hu, and X.-w. Hu, "Principle of using borehole electrode current method to monitor the overburden stratum failure after coal seam mining and its application," *Journal of Applied Geophysics*, vol. 179, article 104111, 2020.

[16] J.-g. Chen, Z.-q. Xiong, H. Li et al., "Failure characteristics of floor under predssure inclined and extra thick coal seam in full-mechanized top coal caving faces," *Chinese Journal of Rock Mechanics and Engineering*, vol. 35, no. S1, pp. 3018–3023, 2016.

[17] Y. Ou, P. Zhang, M. Fu et al., "Geoelectric field response characteristics analysis of floor roadway surrounding rock fracture caused due to coal seam mining," *Scientific Reports*, vol. 11, no. 1, pp. 1–15, 2021.

[18] W.-l. Zhou, P.-s. Zhang, R.-x. Wu, and X.-y. Hu, "Dynamic monitoring the deformation and failure of extra-thick coal seam floor in deep mining," *Journal of Applied Geophysics*, vol. 163, pp. 132–138, 2019.

[19] P.-s. Zhang, C. Liu, Y.-c. Ou, B.-y. Sun, S.-a. Xu, and S.-l. Li, "Comprehensive testing research on floor damage characteristics of mining extra-thick seam in Jungar coalfield," *Coal Geology & Exploration*, vol. 49, no. 1, pp. 263–269, 2021.

[20] G.-j. Zhang and Y. Zhang, "Partition failure characteristics of rock material loading and unloading based on Mohr-Coulomb criterion," *Journal of China coal society*, vol. 44, no. 4, pp. 1049–1058, 2019.

[21] Z.-z. Liang and W.-c. Song, "Theoretical and Numerical Investigations of the Failure Characteristics of a Faulted Coal Mine Floor Above a Confined Aquifer," *Mine Water and the Environment*, vol. 40, pp. 456–465, 2021.

[22] G. X. Xie, J. Z. Li, L. Wang, and Y. Z. Tang, "Mechanical characteristics and time and space evolvement of stress shell in

stope floor stratum," *Journal of China Coal Society*, vol. 43, no. 1, pp. 52–61, 2018.

[23] A. Li, Q. Ma, Y. Lian, L. Ma, Q. Mu, and J. Chen, "Numerical simulation and experimental study on floor failure mechanism of typical working face in thick coal seam in Chenghe mining area of Weibei, China," *Environmental Earth Sciences*, vol. 79, no. 5, pp. 1–22, 2020.

[24] P. Lu, N. Lalam, M. Badar et al., "Distributed optical fiber sensing: Review and perspective," *Applied Physics Reviews*, vol. 6, 35 pages, 2019.

[25] H.-f. Duan, "Analysis on failure features and failure depth of coal seam floor during mining process," *Coal Science and Technology*, vol. 42, no. 5, pp. 17–20, 2014.

[26] J. Chai, Y.-l. Liu, Q. Yuan et al., "Theory-technology and application of optical fiber sensing ondeformation and failure of mine surrounding rock," *Coal Science and Technology*, vol. 49, no. 1, pp. 208–217, 2021.

[27] P.-s. Zhang, J.-w. Wu, and S.-d. Liu, "Study on dynamic observation of coal seam floor's failure law," *Chinese Journal of Rock Mechanics and Engineering*, vol. 2006, no. S1, pp. 3009–3013, 2006.

[28] L.-f. Zhang, D.-x. Yang, Z.-h. Chen, and A. Liu, "Deformation and failure characteristics of sandstone under uniaxial compression using distributed fiber optic strain sensing," *Journal of Rock Mechanics and Geotechnical Engineering*, vol. 12, no. 5, pp. 1046–1055, 2020.

[29] Y.-k. Sun, Q. Li, D.-x. Yang, C.-k. Fan, and A. Sun, "Investigation of the dynamic strain responses of sandstone using multichannel fiber-optic sensor arrays," *Engineering Geology*, vol. 213, pp. 1–10, 2016.

[30] Y.-j. Guo, M. Pan, and F. Yan, "Application of natural neighbor interpolation method in three-dimensional geological modeling," *Journal of PLA University of Science and Technology*, vol. 10, no. 6, pp. 650–655, 2009.

[31] W. Zhang, Q.-y. Qin, and X.-x. Jiang, "Natural neighbor interpolation and its application to 2D grid of irregular data," *Computing Techniques for Geophysical and Geochemical Exploration*, vol. 33, no. 3, p. 294, 2011.